

# Highly sensitive and molecular selective electrochemical sensing of 6-benzylaminopurine with multiwall carbon nanotube@SnS<sub>2</sub>-assisted signal amplification

Tian Gan<sup>1</sup> · Zhen Lv<sup>1</sup> · Yunyun Sun<sup>1</sup> · Zhaoxia Shi<sup>1</sup> · Junyong Sun<sup>1</sup> · Aixia Zhao<sup>1</sup>

Received: 4 August 2015 / Accepted: 4 January 2016 / Published online: 11 January 2016  
© Springer Science+Business Media Dordrecht 2016

**Abstract** A selective and sensitive electrochemical sensor has been prepared for the determination of 6-benzylaminopurine (BAP) in complex matrices. It was fabricated by thoroughly mixing multiwall carbon nanotube@SnS<sub>2</sub> (MWNT@SnS<sub>2</sub>) with molecularly imprinted chitosan (CHIT), and then covering on the surface of glassy carbon electrode (GCE). The core/shell-structured MWNT@SnS<sub>2</sub> dramatically improved the sensitivity of the developed sensor through providing increased binding and preconcentration onto the modified GCE, while CHIT imprinted with BAP served as the selective recognition sites. Several experimental parameters such as pH, amount of modifier,

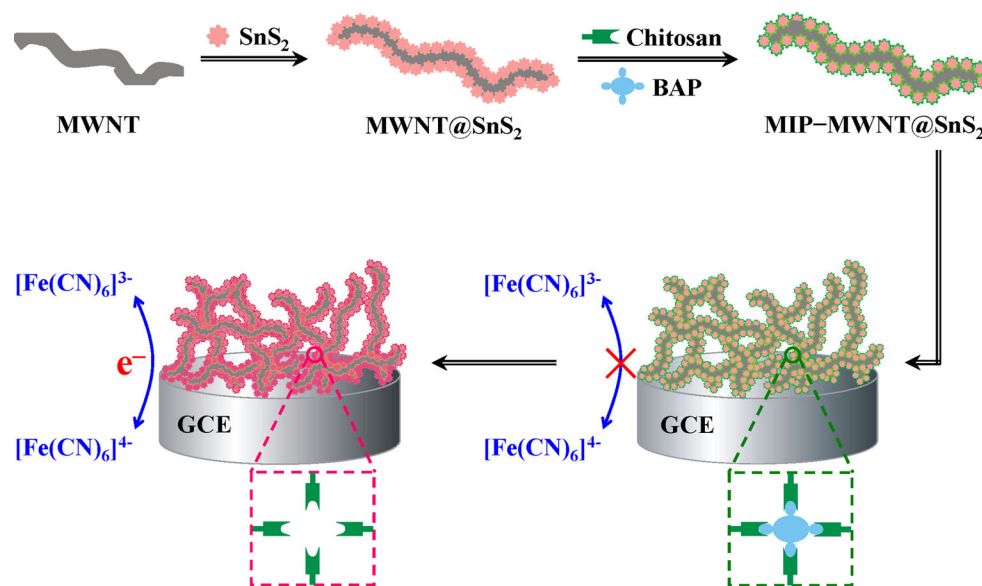
extraction time, and incubation time were optimized. Under the optimal conditions, selective detection of BAP in a linear concentration range of 0.1 nM–10 mM was performed with the detection limit of 50 pM (3S<sub>b</sub>/S). The relative standard deviation of repeatability and reproducibility of the sensor was 1.14 and 2.42 %, respectively. Furthermore, the sensor was successfully applied to the determination of BAP in vegetable and fruit samples, indicating the molecularly imprinted polymer-based electrochemical sensing platform might provide a rapid, sensitive, and cost-effective strategy for BAP determination and related food safety analysis.

---

✉ Tian Gan  
gantianxynu@163.com

<sup>1</sup> College of Chemistry and Chemical Engineering, Xinyang Normal University, Xinyang 464000, China

## Graphical Abstract



**Keywords** Electrochemical sensor · Molecularly imprinted polymer · Multiwall carbon nanotube · SnS<sub>2</sub> · 6-Benzylaminopurine

## 1 Introduction

Pesticides are inevitably essential in modern agriculture, but many experiments and surveys indicate that the abuse of pesticides results in adverse effects not only on the human health but also on the environmental risks [1]. Therefore, the widespread application of pesticides has become a global issue. Among the pesticides, 6-benzylaminopurine (BAP) is identified as the first-generation man-made plant growth regulator, which can be used for the stimulation of plant cell growth and division, basal shoot formation, lateral bud emergence, flowering, and fruit set [2]. Based on these functions, some market traders use excessive BAP in agriculture, horticulture, and fruits growing to improve their organoleptic quality, post-harvest life, and production to achieve high profit. However, an excessive intake of BAP may cause irritation and damage to mucous membranes, eyes, skin, and upper respiratory tract, and some symptoms such as emesis and sicchasia may occur consequently [3]. In this sense, the development of a rapid, sensitive, inexpensive, reliable, on-site detection method for BAP residues in vegetables and fruits is important for concern about food safety. Many methods have been developed for the detection of BAP from food samples [4–10], which generally require high-quality organic solvents, complicated pre-treatments and trained

personnel. This has led to the development of faster and more efficient methods that are both inexpensive and environmentally friendly. In contrast, electrochemical sensors [11–14] have received remarkable attention particularly because of their rapid response, high sensitivity, convenient use, time saving, stability, and low cost, which offer good prospects for meeting the growing needs of food safety detection. Furthermore, electrochemical sensors have received successful application in the field of environmental toxins detection [15–17]. Nonetheless, the sensitivity and selectivity of these electrochemical sensors need further improvement.

During the last two decades, molecular imprinting emerged as a valuable technique and has led to the tremendous research interest from scientists devoting to electrochemical sensor development, owing to its unique advantages including ease of preparation, rapidness, low cost, reusability, long-term stability, and predetermined selectivity [18, 19]. Ye et al. [20], Si and colleagues [21] and Sales and colleagues [22] have testified that the highly selective recognition characteristics of the molecularly imprinted polymers (MIPs) on electrode surface are better than those of natural biological species such as receptors and antibodies. Despite the excellent selectivity of molecularly imprinted electrochemical sensors, the main challenge that still remains to be addressed is their poor sensitivity to template molecules resulted from the poor conductivity of MIPs. Then the researchers have made great efforts to find novel nanomaterials to enhance the sensitivity of molecularly imprinted electrochemical sensors [23].

Compared with other potential nanomaterials, multiwall carbon nanotube (MWNT) with one-dimensional tubular structure is acknowledged to be promising material in the field of electrode modification and electrochemical sensor, owing to a number of fascinating properties such as large surface area, high electrocatalytic activity, great mechanical strength, excellent chemical and physical stabilities, and electronic conductivity [24]. These electrochemical sensors fabricated qualified platforms for the acceleration of electron transfer between target molecules and the electrodes, thus improving the possibility of sensitivity enhancement [25]. However, the large length-to-diameter ratio of MWNT causes it to become easily entangled, which finally influences its properties. One effective strategy to overcome this problem points to the fabrication of core/shell structure with a MWNT core and a hierarchical shell, which can extremely amplify the signal transduction efficiency and yield a dramatic improvement of the sensitivity [26].  $\text{SnS}_2$  is a crucial IV–VI semiconductor material with a layered  $\text{CdI}_2$ -type structure, whose appealing catalytic activity and high electrical conductivity had been demonstrated in lithium batteries [27]. Moreover, because of its environment friendliness and high carrier mobility, the thin layer of  $\text{SnS}_2$  is particularly desirable for nanoelectronics applications [28, 29].

As far as we know, there is no report available in the literature regarding the molecularly imprinted electrochemical sensing of BAP. Herein, a novel electrochemical sensor for the determination of BAP in vegetable and fruit samples was fabricated through the modification of a glassy carbon electrode (GCE) with composite of core/shell-structured MWNT@ $\text{SnS}_2$  and molecularly imprinted chitosan (CHIT). The schematic representation of the possible mechanism of molecular imprinting at the surface

of MWNT@ $\text{SnS}_2$  is illustrated in Scheme 1. The MWNT@ $\text{SnS}_2$  as electrode material was used to significantly increase the electron transfer efficiency and surface area of the sensor, which resulted in an improvement of the sensitivity. Simultaneously, the polymeric film with imprinted sites showed ability to selectively bind BAP target molecules. Finally, MIP-MWNT@ $\text{SnS}_2$  was successfully applied for convenient, rapid, sensitive, and selective detection of trace BAP in vegetable and fruit samples.

## 2 Experimental

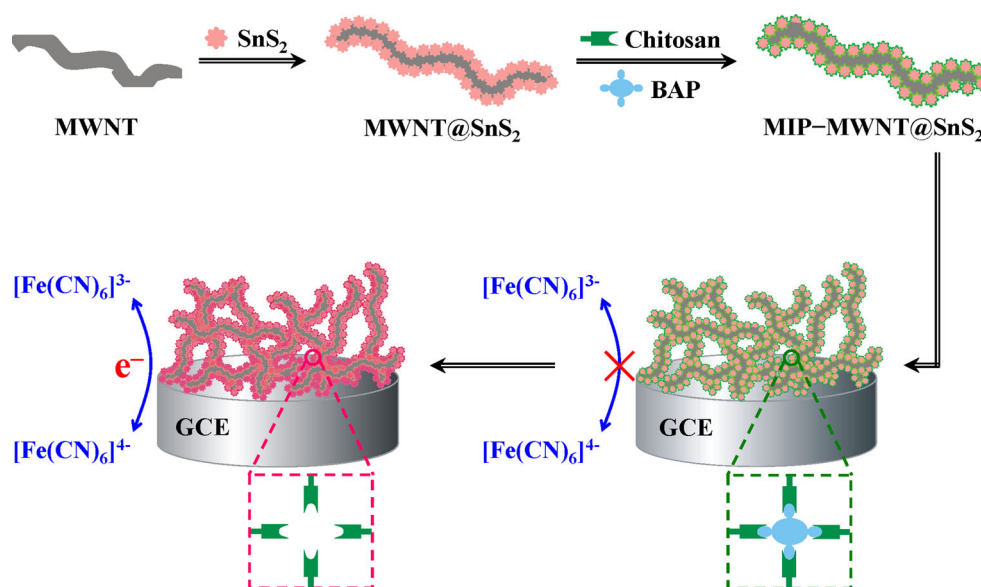
### 2.1 Chemicals and reagents

MWNTs were purchased from Shenzhen Nanotech Port Co., Ltd. (Shenzhen, China) ([www.nanotubes.com.cn](http://www.nanotubes.com.cn)). Tin(IV) chloride pentahydrate ( $\text{SnCl}_4 \cdot 5\text{H}_2\text{O}$ ), thioacetamide (TAA), CHIT, BAP, indole-3-acetic acid (IAA), 6-benzoyloxypurine (BOP), 6-benzylguanine (BG), kinetin (KIN), *m*-topolin (MT), roscovitine (ROSC), olomoucine (OLO), and bohemine (BOH) were obtained from Sigma-Aldrich (China) ([www.sigmaaldrich.com/china](http://www.sigmaaldrich.com/china)). All reagents were of analytical grade and used without further purification. Stock solution of 0.01 M BAP was prepared with absolute ethanol and diluted before the measurements.

### 2.2 Instrumentation

Electrochemical measurements were performed using an CHI 660D electrochemical workstation (Shanghai, China), and the data were recorded using a conventional three-electrode system with a MIP-MWNT@ $\text{SnS}_2$ -modified

**Scheme 1** A schematic illustration for the molecular imprinting mechanism on MIP-MWNT@ $\text{SnS}_2$ /GCE



GCE as working electrode, Pt wire as counter electrode, and saturated calomel electrode as reference electrode. X-ray diffraction (XRD) analysis was carried out using a Rigaku TTR-III X-ray diffractometer, with the Cu K $\alpha$  radiation ( $\lambda = 1.5406 \text{ \AA}$ ) as the X-ray source and a monochromator, positioned in front of the detector. Scanning was performed over a  $2\theta$  angle ranging from  $10^\circ$  to  $70^\circ$  with a speed of  $2^\circ \text{ min}^{-1}$  and step rise of 0.05. Raman spectrum (Renishaw inVia Raman microscope) was recorded on the condition of 514 nm Ar ion laser excitation at 6 mW for 50 s. Energy-dispersive X-ray (EDX) spectrum and field emission scanning electron micrographs (SEMs) were obtained using a Hitachi S-4800 microscope. Field emission transmission electron microscopy (TEM) characterizations were performed on a Tecnai G2 20 S-twin transmission electron microscope operating at 200 kV, for which each sample was prepared by dispersing it in ethanol and drop-casting onto a 200 mesh copper grid coated with holey carbon.

Liquid chromatography-tandem mass spectrometry (LC–MS) method was employed for comparison purpose [4]. A chromatography apparatus, Agilent 1200 (Agilent Technologies, Santa Clara, CA, USA), consists of an autosampler module, a degasser, a binary pump, a column heater/selector and a MS detector from the same provider was used. The column was an Agilent XDB-C18 (1.8  $\mu\text{m}$ , 50 mm  $\times$  4.6 mm). The mass detection was achieved with an LTQ XL ion trap (Thermo Fischer Scientific, San Jose, CA, USA), equipped with heated electrospray ionization (HESI-II) probe.

### 2.3 Preparation of MWNT@SnS<sub>2</sub>

First, the MWNT was acid-treated according to previous report [30]. 1.0 g of MWNT was refluxed in 30 mL HNO<sub>3</sub> (65 wt%) at 140 °C for 6 h. After being rinsed with large amount of water to a neutral pH values, the MWNT was collected by filtration and dried at 60 °C for further use. In a typical procedure of MWNT@SnS<sub>2</sub> [31], 0.05 g acid-treated MWNTs were added to 10 mL absolute ethanol and the MWNTs were well dispersed by completely volatilizing the ethanol through violent ultrasonication. Then, 40 mL distilled water, 1.05 g SnCl<sub>4</sub>·5H<sub>2</sub>O, and 2.25 g TAA were added to the MWNTs successively at room temperature. The resultant mixture was continually stirred at 25 °C for 1 h and then transferred to a Teflon-lined stainless-steel autoclave (capacity of 80 mL). The autoclave was sealed and maintained at 100 °C for 4 h. The system was then cooled to ambient temperature naturally. The final product was collected and washed with ethanol and distilled water for six times, followed by vacuum drying. The SnS<sub>2</sub> was also prepared according to the above procedures without the addition of MWNTs. A suspension

containing 20 mg MWNT, SnS<sub>2</sub>, or MWNT@SnS<sub>2</sub> and 10 mL water was prepared by ultrasonication for 2 h.

### 2.4 Sensor fabrication

A bare GCE with diameter of 3 mm was sequentially polished on micro-cloth pads using 0.1 and 0.05  $\mu\text{m}$  alumina slurries until a mirror-like surface was achieved. Then, the GCE was thoroughly rinsed with water and consecutively sonicated for 1 min in ethanol/water (1:1, v/v) and water, the electrode was dried at room temperature.

CHIT solution was prepared by dissolving 100 mg CHIT in 10 mL aqueous acetic acid (1 wt%) at room temperature. Afterward, 1.0 mL of 15 mM BAP was mixed with 1 mL CHIT solution and 1 mL MWNT@SnS<sub>2</sub> suspension by ultrasonic agitation for 30 min, followed by magnetic stirring for 1 h. A black and homogeneous solution of BAP–CHIT–MWNT@SnS<sub>2</sub> was obtained. 4  $\mu\text{L}$  of the solution was spread evenly on the surface of a GCE with a syringe and allowed to evaporate water in air to form BAP–CHIT–MWNT@SnS<sub>2</sub>/GCE. Finally, the MIP–MWNT@SnS<sub>2</sub>/GCE was obtained by immersing BAP–CHIT–MWNT@SnS<sub>2</sub>/GCE in absolute ethanol for 40 min to completely remove the BAP molecules, creating the specific-binding cavities. As a control, non-imprinted polymer sensor (NIP–MWNT@SnS<sub>2</sub>/GCE) was also fabricated using the same procedure mentioned above, but excluding BAP from the CHIT solution. In order to exhibit the unique properties of MWNT@SnS<sub>2</sub>, the imprinted CHIT film modified GCE (MIP/GCE) was also prepared. These electrodes were stored at room temperature before use.

### 2.5 Preparation and determination of vegetable and fruit samples

Vegetable samples (soybean sprout, mung bean sprout, potato, and tomato) and fruit samples (pear and apple) were obtained from the local markets. Five gram of each sample was homogenized and extracted with 25 mL ethyl alcohol with ultrasonic treatment for 30 min [32]. Then, the supernatants were taken, filtered through a 0.45  $\mu\text{m}$  membrane, and finally concentrated to 5.0 mL. The obtained sample extracts were stored at 4 °C before being determined by this sensor and LC–MS method directly. The concentration of BAP in these samples could be obtained from standard addition method.

### 2.6 Electrochemical measurements

The cyclic voltammetry (CV) and electrochemical impedance spectroscopy (EIS) were carried out in 2.0 mM

$\text{K}_3\text{Fe}(\text{CN})_6$  as a probe in 0.2 M PBS (pH 6.5). The cyclic voltammograms were recorded between  $-0.2$  and  $0.6$  V at a scan rate of  $100 \text{ mV s}^{-1}$ . The impedance measurements were carried out at a potential of  $0.2$  V over the frequency ranging from  $0.1$  Hz to  $100$  kHz, using an alternating voltage of  $2$  mV. The differential pulse voltammetry (DPV) measurements were performed in 0.2 M PBS (pH 6.5) containing  $0.5 \text{ mM K}_3\text{Fe}(\text{CN})_6$  in a potential range of  $-0.2$  to  $-0.5$  V, a amplitude of  $50$  mV, a pulse width of  $0.2$  s, and a pulse period of  $0.5$  s. All experiments were conducted at room temperature. All experiments were performed in sextuplicate, and curves were fitted by using the average values of all replicates.

### 3 Results and discussion

#### 3.1 Characterization of MWNT@SnS<sub>2</sub>

The surface composition of the MWNT@SnS<sub>2</sub> was analyzed by EDX. The result shown in Fig. 1a reveals that C, Sn, and S coexist in the product. According to the integral area of Sn–S, the atomic ratio of Sn/S is about 1:2.1, which is close to stoichiometric ratio of pure SnS<sub>2</sub>.

The crystalline phases of the as-prepared MWNT@SnS<sub>2</sub> were confirmed with XRD (Fig. 1b). The strong peak locates at  $2\theta = 26.05^\circ$  and a weak peak locates at  $2\theta = 42.77^\circ$  are observed and, respectively, correspond to the (002) and (100) diffraction patterns of typical graphite [33], which indicate that the MWNT keeps well graphitization degree after the coverage of SnS<sub>2</sub>. Moreover, seven diffraction peaks are also observed at  $2\theta$  of  $14.81^\circ$ ,  $28.55^\circ$ ,  $31.89^\circ$ ,  $50.29^\circ$ ,  $52.32^\circ$ ,  $56.03^\circ$ , and  $58.79^\circ$  corresponding to the (001), (100), (101), (110), (111), (103), and (201) reflections of the hexagonal crystalline SnS<sub>2</sub> with lattice constants  $a = 3.649$ ,  $c = 5.899 \text{ \AA}$  [34], which are in good agreement with the values in the standard card (JCPDS no. 23-0677). This product has a high purity because no impurity peaks are observed, which is in accordance with the EDX analysis.

Raman measurement is a simple and powerful technique for confirmation of the formation of MWNT@SnS<sub>2</sub> structure. In the typical Raman spectrum of Fig. 1c, the peaks near  $1350$  and  $1581 \text{ cm}^{-1}$  are the D and G bands, respectively. The D band is related to disordered  $\text{sp}^2$ -hybridized carbon atoms containing vacancies, or other symmetry-breaking defects. And the G band is related to graphite  $E_{2g}$  symmetry of the interlayer mode reflecting structural integrity of  $\text{sp}^2$ -hybridized carbon atoms. Furthermore, the extent of carbon-containing defects can be evaluated by the intensity ratio of G band–D band ( $I_G/I_D$ ) [35]. Therefore,  $\text{HNO}_3$  treatment results in high-purity MWNT by removing amorphous carbon and metallic impurities from the

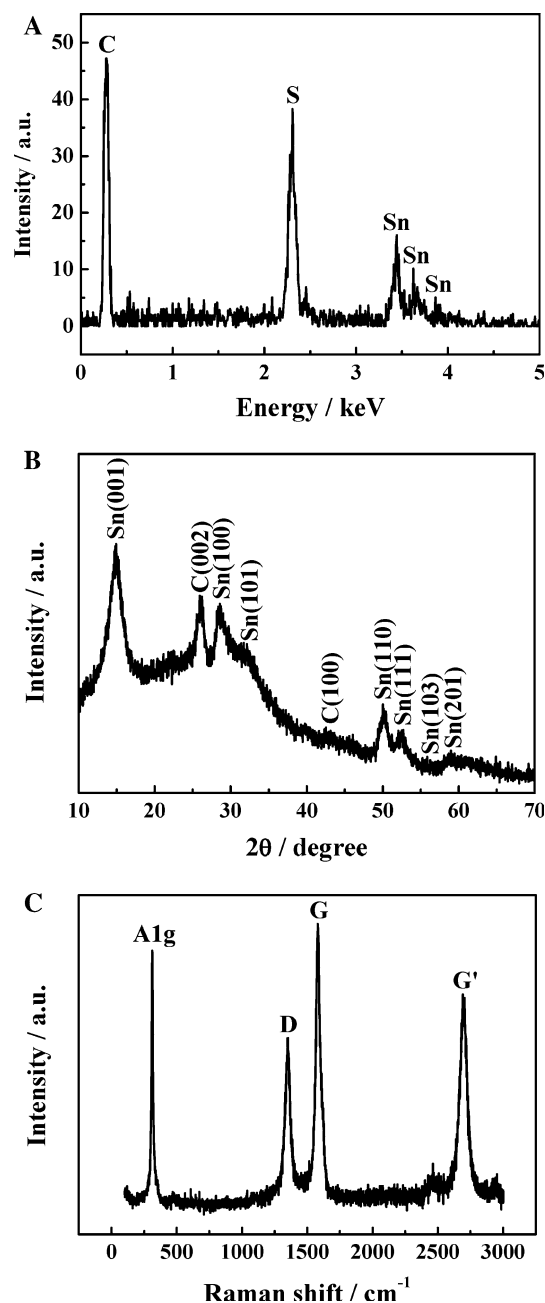


**Fig. 1** EDX analysis (a), XRD pattern (b), and Raman spectrum (c) of MWNT@SnS<sub>2</sub>

purchased MWNT. This is further testified by the presence of strong 2D band at about  $2697 \text{ cm}^{-1}$  in the MWNT@SnS<sub>2</sub>, because the 2D band is originated from the two-photon elastic scattering process, which is always used as an indication of the purity of carbon nanotube. In addition, a strong peak at  $311 \text{ cm}^{-1}$  corresponds to A1g mode that appears in the MWNT@SnS<sub>2</sub> spectrum [36], indicating the formation of SnS<sub>2</sub> on MWNT surface.

The morphology of the MWNT@SnS<sub>2</sub> was observed using SEM. Figure 2a certainly indicates that the high-



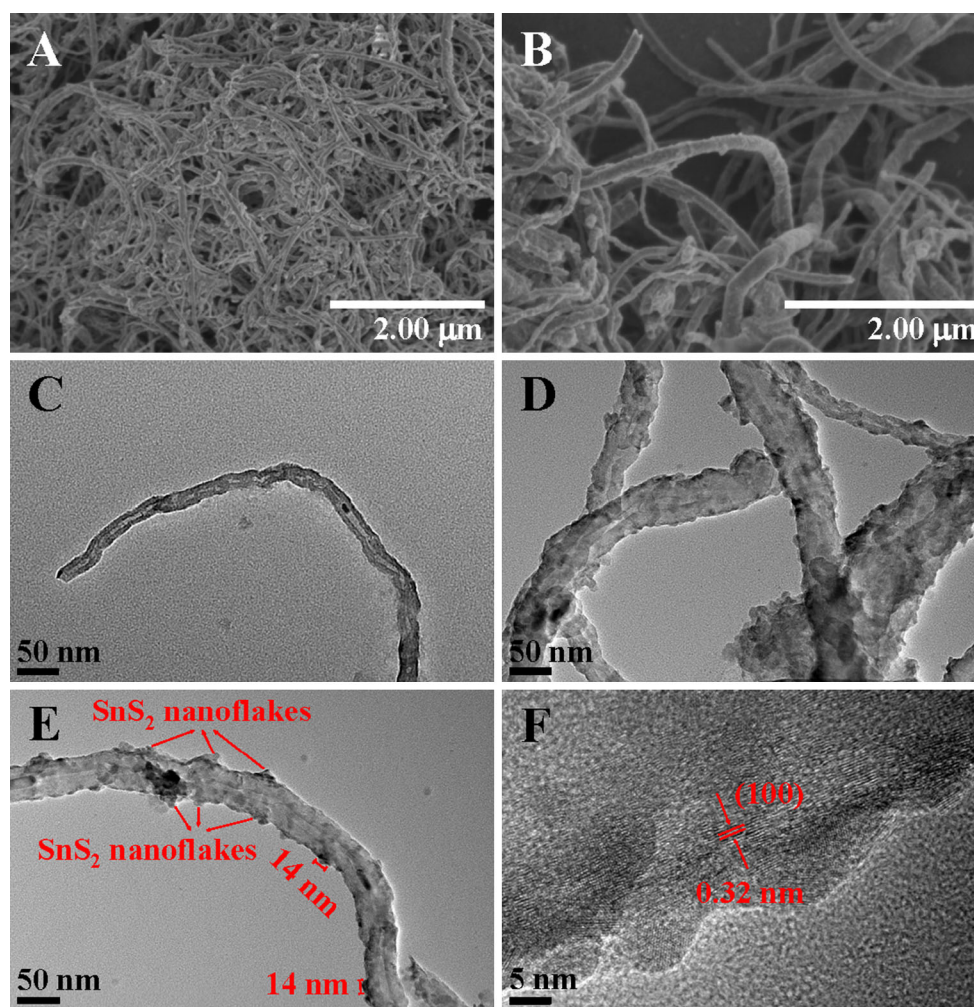


**Fig. 2** a, b SEM images of MWNT@SnS<sub>2</sub>. c TEM image of MWNT. d–f TEM image of MWNT@SnS<sub>2</sub>

structured MWNT@SnS<sub>2</sub> nanotubes form a dense network. The encapsulation of MWNT with SnS<sub>2</sub> shell is clearly shown in Fig. 2b, which displays the good distribution of MWNT in the SnS<sub>2</sub> matrix without any agglomeration. The SnS<sub>2</sub> coating appears to be quite uniform, which may help to separate the MWNT in the final compound due to their large scale.

TEM micrographs of the acid-treated MWNT and MWNT@SnS<sub>2</sub> are presented in Fig. 2c–f. Consistent with the manufacture provided data, the acid-treated MWNT (Fig. 2c) consist of long individual tubes with diameters ranging from 18 to 25 nm, up to micrometer lengths and smooth surface. Almost no trace of other carbon impurities is detected. After surface modification of MWNT with SnS<sub>2</sub>, the diameters of the MWNT increase to 54–61 nm (Fig. 2d), providing evidence that SnS<sub>2</sub> is successfully loaded on the surface of MWNT. Moreover, the MWNT do not suffer any structure destruction after being modified with SnS<sub>2</sub>. Therefore, outstanding physicochemical

properties of MWNT can be maintained after surface modification. The TEM image in Fig. 2e shows the SnS<sub>2</sub> nanoflakes with about 14 nm are dispersed uniformly on the outer MWNT walls. The close interaction between SnS<sub>2</sub> nanoflakes and MWNT in the contact interface can be found, which will be favorable to enhance the electron transfer rate of the sensor. Figure 2f displays the high-resolution TEM image of the top view of SnS<sub>2</sub> nanoflakes coated on the MWNT surface. It can be seen that the interplanar distance of 0.32 nm is in agreement with the *d*-spacing of (100) planes of the hexagonal SnS<sub>2</sub>.

### 3.2 Electrochemical characterization of the MIP sensor

Cyclic voltammetric behaviors at bare GCE and different modified GCE were recorded in PBS solution (pH 6.5) containing 2.0 mM K<sub>3</sub>Fe(CN)<sub>6</sub> to confirm the stepwise fabrication process of the MIP sensor, the results are shown

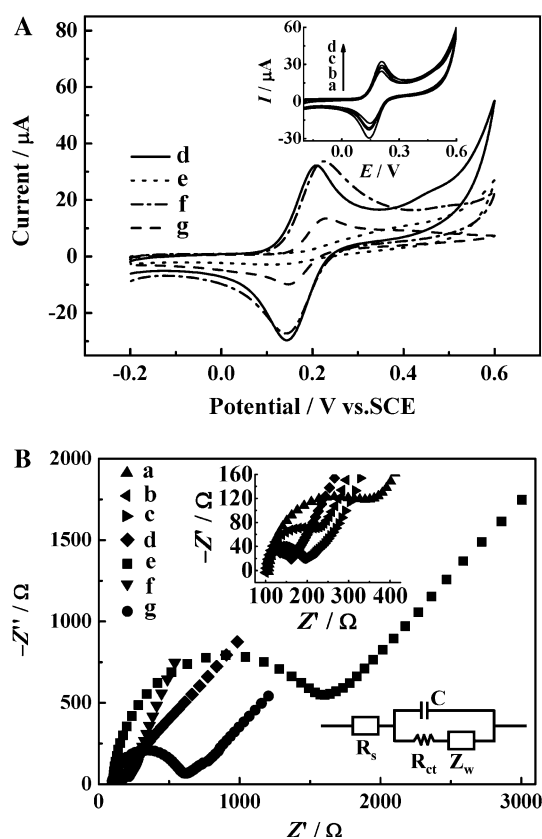


**Fig. 3** Cyclic voltammograms (A) and electrochemical impedance spectra (B) of the bare GCE (a), MWNT/GCE (b), SnS<sub>2</sub>/GCE (c), MWNT@SnS<sub>2</sub>/GCE (d), BAP-CHIT-MWNT@SnS<sub>2</sub>/GCE (e), MIP-MWNT@SnS<sub>2</sub>/GCE (f), and MIP-MWNT@SnS<sub>2</sub>/GCE after incubation in 10 μM BAP (g) in PBS (pH 6.5) containing 2.0 mM K<sub>3</sub>Fe(CN)<sub>6</sub>. Scan rate is 100 mV s<sup>-1</sup>

in Fig. 3A. As observed in curve a, a couple of typical redox peaks attributing to K<sub>3</sub>Fe(CN)<sub>6</sub> appear on the bare GCE, and the change of redox peak currents is used to investigate the change in electrochemical resistance to characterize the electrochemical behavior of MIP sensor. On a MWNT film modified GCE (curve b) and SnS<sub>2</sub> film modified GCE (curve c), the redox peak currents of K<sub>3</sub>Fe(CN)<sub>6</sub> have evident increase. The obvious increase in the redox peak currents demonstrates that an efficient catalytic reaction occurs in the MWNT and SnS<sub>2</sub> film. After the surface of GCE is functionalized with core/shell-structured MWNT@SnS<sub>2</sub>, an increment of redox peak current is seen in curve d when compared with the values at the bare GCE, MWNT/GCE, and SnS<sub>2</sub>/GCE, which can be ascribed to the good electrical conductivity and high surface-to-volume ratio of MWNT@SnS<sub>2</sub> film. Furthermore, the core/shell architecture maximizes the SnS<sub>2</sub>-support interaction through the three-dimensional contact between the SnS<sub>2</sub> nanoflakes and the MWNT, thereby facilitating the electron transfer and thus increasing its rate. Curve e shows the cyclic voltammogram of BAP-CHIT-MWNT@SnS<sub>2</sub>/GCE

in the same solution. The result indicates that the presence of BAP hinders K<sub>3</sub>Fe(CN)<sub>6</sub> from getting access to the surface of GCE, so this modified electrode before template removal is almost non-conductive. After the removal of BAP molecules from BAP-CHIT-MWNT@SnS<sub>2</sub> film through washing the modified electrode with ethanol, the MIP-MWNT@SnS<sub>2</sub>/GCE is obtained and its electrochemical behavior is studied and recorded as curve f. When compared with curve e, the redox peak currents shown in curve f enhance evidently and almost equal to the peak heights in curve d. The embedded BAP molecules that hinder the electron transfer of MIP-MWNT@SnS<sub>2</sub>/GCE are removed, which implies that lots of imprinted cavities are produced in the imprinted membrane. These cavities can be used as channels for the diffusion of [Fe(CN)<sub>6</sub>]<sup>3-/4-</sup> and enhance the redox reaction activity of [Fe(CN)<sub>6</sub>]<sup>3-/4-</sup> ion pair on the MIP sensor surface. In order to investigate the determination of BAP, the process of rebinding was conducted. The curve g in Fig. 3A shows the CV response of the MIP sensor after incubation for 12 min in the presence of BAP at 10 μM. The lower peak currents can be found through a comparison with curve f, attributing to the occupation of imprinted cavities by BAP molecules after rebinding step.

EIS was further used as an efficient tool to investigate the interface properties of modified electrodes. The Nyquist diagrams of various modified electrodes in the presence of 2.0 mM K<sub>3</sub>Fe(CN)<sub>6</sub> in pH 6.5 PBS solution are shown in Fig. 3B. In electrochemical impedance measurements, the electron transfer resistance ( $R_{ct}$ ) during the modification process can be reflected by the semicircle diameter at high frequencies, and a linear part at low frequencies is relative to the diffusion control process. The simple electrical equivalent circuits in the inset of Fig. 3B are used to fit the impedance diagrams. As shown in curve a of Fig. 3B, the bare GCE displays a small semicircle ( $R_{ct} = 327.6 \Omega$ ). In an attempt to find out the effect of core/shell structure on the catalytic activity of MWNT@SnS<sub>2</sub>, the EIS data obtained for MWNT/GCE (curve b), SnS<sub>2</sub>/GCE (curve c), and MWNT@SnS<sub>2</sub>/GCE (curve d) were compared. The results exhibit that  $R_{ct}$  for MWNT/GCE and SnS<sub>2</sub>/GCE are 229.1 and 121.5  $\Omega$ , respectively, much lower than that for bare GCE. After modification of the GCE with MWNT@SnS<sub>2</sub>, an almost straight line in the Nyquist plot is displayed, which corresponds to the characteristic diffusion-limiting process known as Warburg element. The value of  $R_{ct}$  for the MWNT@SnS<sub>2</sub>/GCE is calculated as 81.40  $\Omega$ , which means that the MWNT@SnS<sub>2</sub> core/shell-structured nanocomposite has excellent electric conducting property. Subsequently, when the BAP-imprinted CHIT-MWNT@SnS<sub>2</sub> film is coated on the GCE surface, as shown in curve e, the semicircle of the BAP-CHIT-MWNT@SnS<sub>2</sub>/GCE increases dramatically, and the value

of  $R_{ct}$  increases to 1776  $\Omega$ , indicating that the MIP film before the removal of BAP molecules forms a barrier on the surface of GCE which can block the electron transfer between  $[\text{Fe}(\text{CN})_6]^{3-/4-}$  ion pair and the GCE. The electron transfer resistance of the MIP sensor reduces contrarily ( $R_{ct} = 191.9 \Omega$ ) when the template BAP molecules are removed from the imprinted film (curve f), suggesting that the reserved specific recognition cavities after the removal of template molecules enhance the electron transfer significantly. When BAP molecules are selective rebound on the MIP membrane, as shown in curve g, the  $R_{ct}$  (i.e., 568.9  $\Omega$ ) is higher than that of the MIP-MWNT@SnS<sub>2</sub>/GCE. This can be attributed to the reason that the re-adsorbed BAP molecules on the surface of electrode hinder the electron transfer once again. The results are in accord with that obtained from the CV scanning in Fig. 3A.

### 3.3 Confirmation of BAP molecules in imprinted film

In order to confirm the existence of BAP molecules in imprinted films, DPV of BAP-CHIT/GCE, BAP-CHIT-MWNT@SnS<sub>2</sub>/GCE, MIP-MWNT@SnS<sub>2</sub>/GCE, and NIP-MWNT@SnS<sub>2</sub>/GCE were recorded in the PBS (pH 6.5) solution as a supporting electrolyte, respectively, as shown in Fig. 4. An oxidation peak at 0.98 V, which reveals the typical peak of BAP, can be seen clearly both in curves a and b for BAP-CHIT/GCE and BAP-CHIT-MWNT@SnS<sub>2</sub>/GCE, indicating that BAP molecules have been embedded into the imprinted membrane. As expected, the oxidation peak current in curve b increases significantly compared with curve a, attributing to the core/shell structure of MWNT@SnS<sub>2</sub> nanomaterial, which maximizes the interaction through three-dimensional contact between the MWNT core and the SnS<sub>2</sub> shell, therefore exhibiting

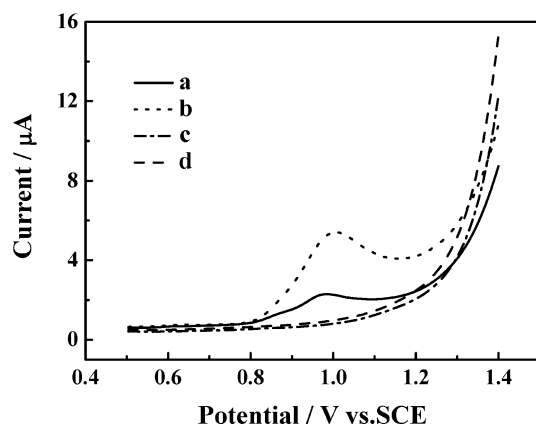


**Fig. 4** Differential pulse voltammograms of BAP-CHIT/GCE (a), BAP-CHIT-MWNT@SnS<sub>2</sub>/GCE (b), MIP-MWNT@SnS<sub>2</sub>/GCE (c), and NIP-MWNT@SnS<sub>2</sub>/GCE (d) in PBS (pH 6.5). Amplitude is 50 mV, pulse width is 0.2 s, and pulse period is 0.5 s

excellent electrocatalytic effect and good conductivity for the electron transportation. Furthermore, the SnS<sub>2</sub> shell offers protection to the MWNT core from coagulation and undoubtedly increases the effective electrode surface area for BAP binding. After immersing into absolute ethanol for 40 min, there is no peak observed for the MIP-MWNT@SnS<sub>2</sub>/GCE (curve c), suggesting that the BAP template molecules embedded in the MIP film can be totally removed by washing with absolute ethanol. In the case of NIP-MWNT@SnS<sub>2</sub>/GCE, no oxidation peak is observed (curve d). The results are ascribed to large amount of recognition cavities for BAP in the MIP-coated MWNT@SnS<sub>2</sub>, while NIP-coated MWNT@SnS<sub>2</sub> has no recognition cavities for binding BAP. The non-printed films were expected to be less porous than the imprinted film, since the extracted template left more cavities and revealed the pores in the film. The porosity enhanced the diffusion of template into the film and could promote the binding within the film.

### 3.4 Optimization of the experimental parameters

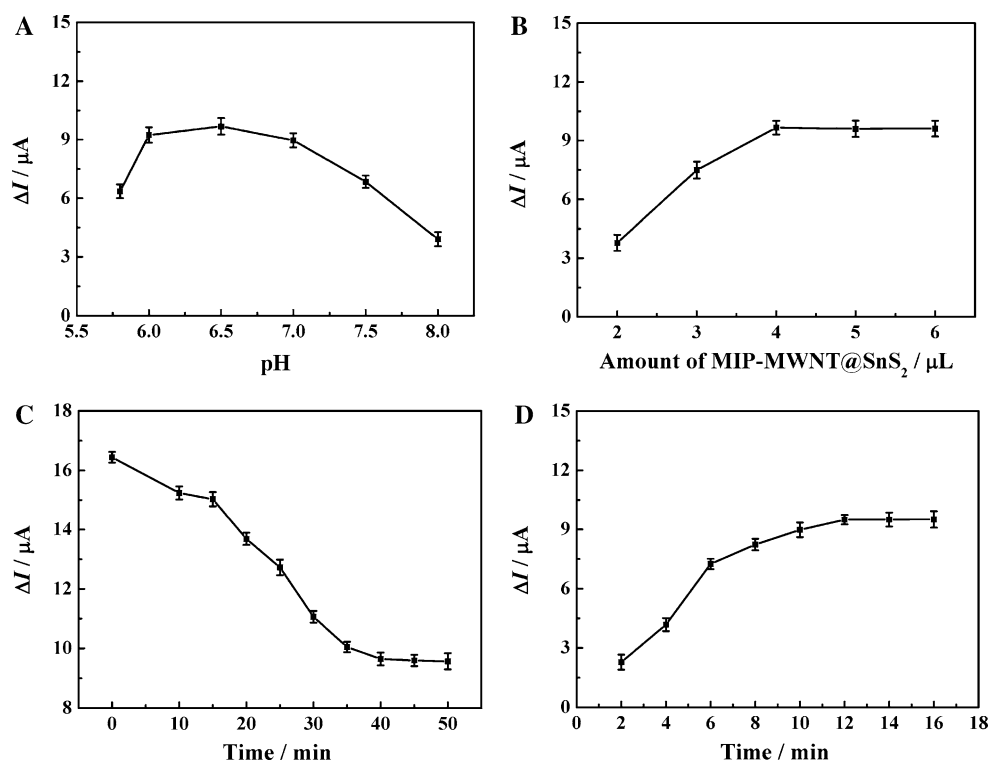
The electrochemical activity of BAP templates is poor, so the “gate-controlled” method with K<sub>3</sub>Fe(CN)<sub>6</sub> as the probe is used here to improve the determination sensitivity. After the extraction of BAP template molecules, the electron transportation of K<sub>3</sub>Fe(CN)<sub>6</sub> can be realized easily using the imprinted cavities as channels. However, some cavities will be blocked by the adsorbed BAP molecules after the rebinding process. Consequently, the electrochemical redox signal derived from the K<sub>3</sub>Fe(CN)<sub>6</sub> system can be controlled by using the extraction and rebinding of BAP template molecules as a switch. By the aid of the “gate-controlled” method, the redox current of K<sub>3</sub>Fe(CN)<sub>6</sub> is indirectly related with BAP template concentration, and the magnified response is achieved. Herein,  $\Delta I = I_0 - I_c$ ,  $I_0$  and  $I_c$  are the currents when the concentrations of BAP are 0 and  $c \mu\text{M}$  in MIP-MWNT@SnS<sub>2</sub> film.

The influence of K<sub>3</sub>Fe(CN)<sub>6</sub> solution with different pH values of 5.8–8.0 on the electrochemical behavior of MIP-MWNT@SnS<sub>2</sub>/GCE toward BAP (10  $\mu\text{M}$ ) was studied with DPV technique. As shown in Fig. 5a, a maximum electrochemical response current is observed at pH 6.5. Thus, pH 6.5 PBS was adopted in subsequent experiments.

The effect of MIP-MWNT@SnS<sub>2</sub> amount was studied in the range of 2–6  $\mu\text{L}$  (Fig. 5b). The electrochemical response current increases when the amount of MIP-MWNT@SnS<sub>2</sub> changes from 2 to 4  $\mu\text{L}$ . Further increase of MIP-MWNT@SnS<sub>2</sub> on electrode surface leads to a gradual decrease of peak current. The imprinted amount of BAP molecules increases with the amount of MIP-MWNT@SnS<sub>2</sub> increasing, and therefore more cavities are produced. But overmuch MIP-MWNT@SnS<sub>2</sub> on electrode surface results



**Fig. 5** Effects of pH (a), amount of MIP-MWNT@SnS<sub>2</sub> (b), extraction time (c), and incubation time (d) on  $\Delta I$  of MIP-MWNT@SnS<sub>2</sub>/GCE



in the increase of resistance and the reduction of electrochemical response current. Furthermore, the template molecules are difficult to be removed completely from the excessively thick MIP membrane. Therefore, 4  $\mu\text{L}$  MIP-MWNT@SnS<sub>2</sub> was a balanced point and was modified on the GCE surface.

Only if the template molecules are removed completely from the imprinted film, high sensitivity, selectivity, and reproducibility of the sensor can be obtained. Various eluents including methanol, ethanol, acetic acid, and their mixture were optimized for removing BAP from the imprinted film because H-bond is the main binding force that combines the imprinted film and BAP template molecules. The results reveal that the BAP molecules are prone to remove completely and the imprinted cavities can maintain integrity and stability when the ethanol is used as eluent. Therefore, absolute ethanol was chosen as the optimum eluent for BAP template removal. Furthermore, the extraction time was investigated (Fig. 5c). The value for  $I_c$  gradually increases and reaches a maximum at about 40 min and then remains stable over 10 min, which means that the BAP template molecules are washed out at about 40 min in the absolute ethanol. As a result, an extraction time of 40 min was selected for all subsequent analysis.

The influence of incubation time on the electrochemical response current was also considered in the range of 2–16 min (Fig. 5d). It is found that the electrochemical response current increases gradually when extending

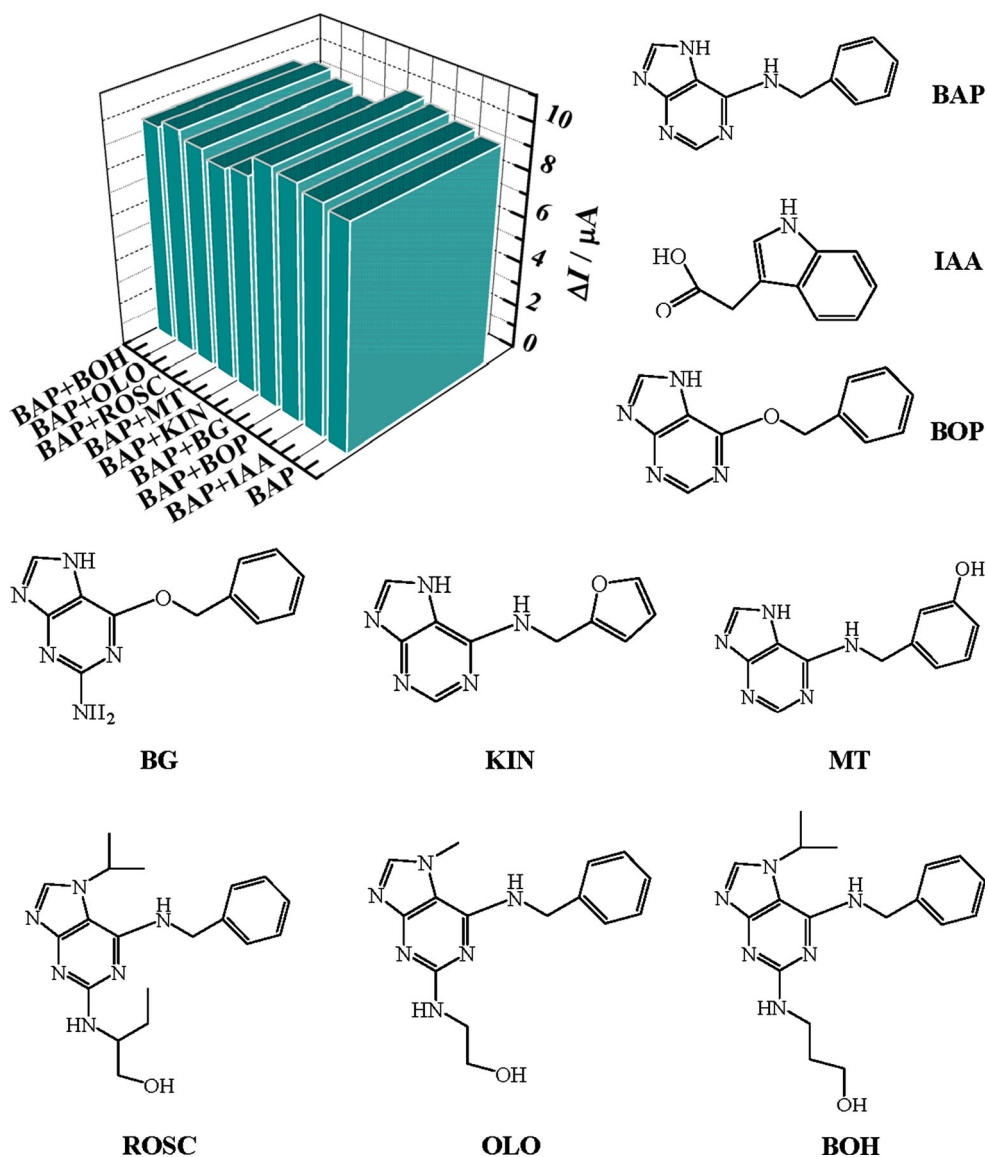
incubation time from 2 to 12 min. Then it keeps almost unchanged, which indicates the re-adsorption of BAP is saturated. Thus, 12 min was chosen as incubation time so that the BAP solutions had enough time to reach saturated adsorption.

### 3.5 Selectivity, repeatability, reproducibility, and stability of the MIP-based electrochemical sensor

The selectivity of MIP-MWNT@SnS<sub>2</sub>/GCE was checked with some analogs, such as IAA, BOP, BG, KIN, MT, ROSC, OLO, and BOH were chosen as objective molecules to study their influence on this MIP-based electrochemical sensor. As shown in Fig. 6, 10-fold concentration of IAA, BOP, BG, KIN, MT, ROSC, OLO, and BOH hardly cause any evident change of peak current for the MIP-MWNT@SnS<sub>2</sub>/GCE (signal change <5%), indicating a good selectivity of this MIP film for BAP.

The repeatability of this MIP sensor was investigated at a BAP concentration of 10  $\mu\text{M}$  with the same MIP-MWNT@SnS<sub>2</sub>/GCE. The relative standard deviation (RSD) of 1.14% for 10 DPV measurements is calculated, which indicates the satisfactory repeatability of the sensor. Additionally, 10 repeated MIP-MWNT@SnS<sub>2</sub>/GCEs were prepared under the same conditions, and the reproducibility was also studied after incubation of the MIP-MWNT@SnS<sub>2</sub>/GCE in 10  $\mu\text{M}$  BAP. The RSD was

**Fig. 6** DPV responses on MIP-MWNT@SnS<sub>2</sub>/GCE for 1.0 μM BAP present in binary mixture (1:1) with structural analogs: indole-3-acetic acid (IAA), 6-benzoyloxypurine (BOP), 6-benzylguanine (BG), kinetin (KIN), *m*-topolin (MT), roscovitine (ROSC), olomoucine (OLO), and bohemine (BOH)



calculated to be 2.42 %, implying acceptable interelectrode reproducibility. In order to evaluate the stability of this MIP sensor, it was stored at room temperature over 20 days, and no significant change of peak current was observed in the same experimental condition. It retained 96.8 % of its original response. Moreover, the response of MIP film for BAP hardly changed after 5 min of ultrasonication. All measurements show the excellent stability of this MIP sensor.

### 3.6 Electrochemical detection of BAP

Under the optimized conditions for the proposed MIP sensor, differential pulse voltammograms of BAP with different concentrations were recorded at the MIP-MWNT@SnS<sub>2</sub>/GCE. Figure 7 shows the dependence of the electrochemical

response on the concentrations of BAP. Owing to the occupation of imprinted cavities by BAP template molecules, the  $I_c$  decreases with the increasing BAP concentrations, and inclines to be stable at high concentration of BAP. The inset of Fig. 7 displays that the  $\Delta I$  is linear with logarithm of BAP concentration over a range from 0.1 nM to 10 mM with the regression equation:  $\Delta I (\mu A) = 8.007 + 1.351 \log c$  (unit of  $c$ ,  $\mu M$ ) ( $r^2 = 0.996$ ). The detection limit is 50 pM based on the  $3S_b/S$  rules [37], where  $S_b$  represents the standard deviation of the peak currents of the bland solution ( $n = 6$ ) and  $S$  represents the slope of the calibration curve for BAP. The electrochemical methods for the determination of BAP have been summarized in Table 1. Compared with the other electrochemical sensors for the assay of BAP, the excellent sensitivity and wide linear range are observed for this proposed sensor.

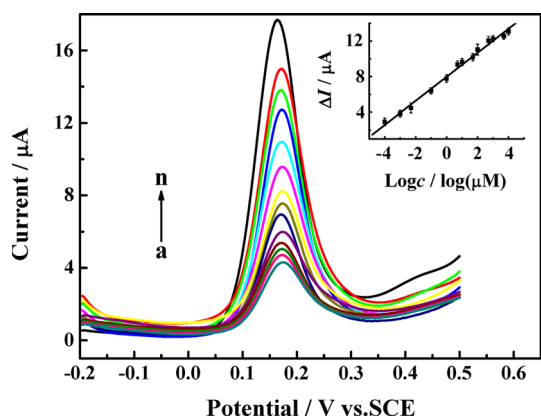


**Fig. 7** Differential pulse voltammograms of 0.5 mM  $K_3Fe(CN)_6$  in pH 6.5 PBS at the MIP-MWNT@SnS<sub>2</sub>/GCE after interaction with different concentrations of BAP solution. Concentration of BAP (from a to n): 0, 0.1 nM, 1.0 nM, 5.0 nM, 0.1 μM, 1.0 μM, 5.0 μM, 10 μM, 50 μM, 0.1 mM, 0.5 mM, 1.0 mM, 5.0 mM, and 10 mM. Other conditions are as in Fig. 4

### 3.7 Determination of BAP in real samples

In order to study the practical applicability of the proposed MIP sensor, the content of BAP in vegetable and fruit samples including soybean sprout, mung bean sprout, potato, tomato, pear, and apple was analyzed, and the results are shown in Table 2. BAP in different samples was detected with the MIP-MWNT@SnS<sub>2</sub>/GCE based on standard addition method. Each sample was determined for six times and the RSD was not higher than 3 %, revealing

good precision. The results were also compared using LC–MS and are also tabulated in Table 2. The results show that the two methods are in good agreement and the MIP-MWNT@SnS<sub>2</sub>/GCE can be used for accurate determination of BAP in these samples. Otherwise, the average recovery of the MIP-MWNT@SnS<sub>2</sub>/GCE toward BAP in these samples ranges from 91.0 to 103 %, validating the good recovery and practicability of the developed MIP sensor.

## 4 Conclusions

In conclusion, the development of a simple molecular imprinting procedure to prepare a BAP-imprinted voltammetric sensor based on a GCE modified with molecularly imprinted CHIT-MWNT@SnS<sub>2</sub> composite film was described here. Due to the excellent electrocatalytic activity and high conductivity of MWNT@SnS<sub>2</sub> and the selective recognition of CHIT with BAP, the prepared sensor exhibited enhanced response for the electrochemical oxidation of BAP. This sensing platform not only showed significant improved sensitivity by the strategy of gate-controlled electrocatalytic effect, but also offered the advantages of convenience, long-term stability, and efficient assay in target detection, which were essential for the BAP detection in food safety monitoring. Moreover, this strategy was employed to detect BAP in vegetable and fruit samples successfully, which could further be expected to

**Table 1** Comparison of different electrodes for the determination of BAP

Modified electrodes	Linear ranges	Limit of detection	References
Carbon nanotube/GCE	40 nM–10 μM	5.0 nM	[18]
Carbon nanotube-dicetyl phosphate/GCE	50 nM–2.5 μM	20 nM	[19]
Acetylene black–dihexadecyl hydrogen phosphate/GCE	20 nM–5 μM	5.0 nM	[20]
Pt/ordered mesoporous carbons/GCE	50 nM–24 μM	5.0 nM	[21]
MIP-MWNT@SnS <sub>2</sub> /GCE	0.1 nM–10 mM	50 pM	This work

**Table 2** Detection and recovery of BAP in vegetables and fruits

Samples	Detection				Recovery test		
	By this sensor (μM)	RSD (%)	By LC–MS (μM)	Relative error (%)	Spiked (μM)	Found (μM)	Recovery (%)
Soybean sprout	2.58	1.6	2.54	1.6	3.00	2.42	93.7
Mung bean sprout	5.25	1.7	5.31	−1.1	5.00	4.75	95.0
Potato	0.186	3.0	0.182	2.2	0.200	0.182	91.0
Tomato	0.0504	3.0	0.0511	−1.4	0.0500	0.0513	103
Pear	0.692	2.3	0.688	0.58	0.700	0.684	97.7
Apple	0.463	2.4	0.452	2.4	0.500	0.508	102

be used in fabrication of various MIP-based electrochemical sensors by replacing BAP with other template molecules for chemical/biological detections.

**Acknowledgments** The authors gratefully acknowledge the financial support from the National Science Foundation of China (No. 61201091), the Program for University Key Scientific Research of Henan (No. 15A150025), the Program for University Innovative Research Team of Henan (No. 15IRTSTHN001), and the Key Scientific and Technological Project of Henan (No. 152102210341). The Center of Analysis and Testing of Xinyang Normal University was also acknowledged for its help in the EDX, SEM, and TEM observation.

## References

- Bui MPN, Seo SS (2015) Electrochemical analysis of parathion-ethyl using zirconium oxide-laponite nanocomposites-modified glassy carbon electrode. *J Appl Electrochem* 45:365–373. doi:10.1007/s10800-015-0789-0
- Barclay GF, McDavid CR (1998) Effect of benzylaminopurine on fruit set and seed development in pigeonpea. *Sci Hortic Amst* 72:81–86. doi:10.1016/S0304-4238(97)00110-6
- Li X, Chen X, Yao X, Jin M, Jiang J (2005) Determination of 6-benzylaminopurine in bean-sprout by high performance liquid chromatography. *Chin J Health Lab Technol* 15:149–151. doi:10.3969/j.issn.1004-8685.2005.02.010
- Zhang YL, Liu H, Wang SL, Ding T, Xu NS, Yu KY, Shen WJ, Zhao ZY, Liu Y, Wu B, Zhang R, Shen CY (2015) Simultaneous determination of eight kinds of drug residues in sprouts by high performance liquid chromatography–tandem mass spectrometry. *J Instrum Anal* 34:164–170. doi:10.3969/j.issn.1004-4957.2015.02.007
- Qiao M, Liu SP, Liu ZF, Yang JD, Zhu JH, Hu XL (2014) Overlapping of second order scattering and frequency double scattering spectra method and resonance Rayleigh scattering method for the determination of 6-benzyladenine in bean sprout. *Food Anal Methods* 7:1737–1744. doi:10.1007/s12161-014-9812-z
- Wu PG, Tan Y, Zhang J, Wang LY, Tang J, Jiang W, Pan XD, Ma BJ, Ni ZN, Wang TJ (2014) Determination of 10 plant growth regulators in bean sprouts by sequential cleaning-gas chromatography–mass spectrometry. *Chin J Anal Chem* 42:866–871. doi:10.3724/SP.J.1096.2014.40105
- Zhao XH, Feng XM, Zhu QH, Yang Q, Li XY, Zhang J (2014) Determination of kinetin and 6-benzylaminopurine in fruits and vegetables based on L-Phe fluorescence quenching. *Jiangsu J Agric Sci* 30:880–884. doi:10.969/j.issn.1000-4440.2014.04.030
- Lee S, Kim GY, Moon JH (2013) Detection of 6-benzylaminopurine plant growth regulator in bean sprouts using OFRR biosensor and QuEChERS method. *Anal Methods* 5:961–966. doi:10.1039/c2ay26136g
- Zhang P, Zheng DW, Liu J, Zhong RG, Liu CW, Guo X, Wang H (2012) Rapid detection of 6-benzylaminopurine residues in sprout beans by surface-enhanced Raman spectroscopy. *Spectrosc Spectr Anal* 32:1266–1269. doi:10.3964/j.issn.1000-0593(2012)05-1266-04
- Assuncao NA, Arruda SCC, Martinelli AP, Carrilho E (2009) Direct determination of plant-growth related metabolites by capillary electrophoresis with spectrophotometric UV detection. *J Braz Chem Soc* 20:183–187. doi:10.1590/S0103-50532009000100027
- Zhao G, Liu KZ, Lin S, Liang J, Guo XY, Zhang ZJ (2003) Application of a carbon nanotube modified electrode in anodic stripping voltammetry for determination of trace amounts of 6-benzylaminopurine. *Microchim Acta* 143:255–260. doi:10.1007/s00604-003-0078-1
- Li CY (2006) Electrochemical determination of 6-benzylaminopurine (6-BAP) using a single-wall carbon nanotube-dicetyl phosphate film coated glassy carbon electrode. *Bull Korean Chem Soc* 27:991–994. doi:10.5012/bkcs.2006.27.7.991
- Sun D, Zhang HJ (2006) Voltammetric determination of 6-benzylaminopurine (6-BAP) using an acetylene black–dihexadecyl hydrogen phosphate composite film coated glassy carbon electrode. *Anal Chim Acta* 557:64–69. doi:10.1016/j.aca.2005.10.002
- Zhang YF, Bo XJ, Guo LP (2012) Electrochemical behavior of 6-benzylaminopurine and its detection based on Pt/ordered mesoporous carbons modified electrode. *Anal Methods* 4:736–741. doi:10.1039/C2AY05712C
- Rahman LU, Shah A, Khan SB, Asiri AM, Hussain H, Han C, Qureshi R, Ashiq MN, Zia MA, Ishaq M, Kraatz HB (2015) Synthesis, characterization, and application of Au–Ag alloy nanoparticles for the sensing of an environmental toxin, pyrene. *J Appl Electrochem* 45:463–472. doi:10.1007/s10800-015-0807-2
- Rahman LU, Shah A, Qureshi R, Khan SB, Asiri AM, Shah AUHA, Ishaq M, Khan MS, Lunsford SK, Zia MA (2015) Spectroscopic analysis of Au–Cu alloy nanoparticles of various compositions synthesized by a chemical reduction method. *Adv Mater Sci Eng*. doi:10.1155/2015/638629
- Rahman LU, Shah A, Lunsford SK, Han C, Nadagouda MN, Sahle-Demessie E, Qureshi R, Khan MS, Kraatz HB, Dionysiou DD (2015) Monitoring of 2-butanone using a Ag–Cu bimetallic alloy nanoscale electrochemical sensor. *RSC Adv* 5:44427–44434. doi:10.1039/c5ra03633j
- Huang JD, Zhang XM, Liu S, Lin Q, He XR, Xing XR, Lian WJ (2011) Electrochemical sensor for bisphenol A detection based on molecularly imprinted polymers and gold nanoparticles. *J Appl Electrochem* 41:1323–1328. doi:10.1007/s10800-011-0350-8
- Wang YY, Ya Y, Tan XH, Huang KJ, Li CY (2010) Investigation on electrochemical preparation of methyl parathion imprinted film modified electrode and its application. *J Xinyang Norm Univ (Nat Sci Ed)* 23:566–570. doi:10.3969/j.issn.1003-0972.2010.01.018
- Ye J, Chen Y, Liu Z (2014) A boronate affinity sandwich assay: an appealing alternative to immunoassays for the determination of glycoproteins. *Angew Chem Int Ed* 53:10386–10389. doi:10.1002/anie.201405525
- Zhang CJ, Si SH, Yang ZP (2015) Design of molecularly imprinted TiO<sub>2</sub>/carbon aerogel electrode for the photoelectrochemical determination of atrazine. *Sens Actuators B* 211:206–212. doi:10.1016/j.snb.2015.01.079
- Moreira FTC, Sharma S, Dutra RAF, Noronha JPC, Cass AEG, Sales MGF (2015) Detection of cardiac biomarker proteins using a disposable based on a molecularly imprinted polymer grafted onto graphite. *Microchim Acta* 182:975–983. doi:10.1007/s00604-014-1409-0
- Justino CIL, Freitas AC, Pereira R, Duarte AC, Santos TAPR (2015) Recent developments in recognition elements for chemical sensors and biosensors. *Trends Anal Chem* 68:2–17. doi:10.1016/j.trac.2015.03.006
- Liu YX, Wang WW, Wei H, Li JW, Lu XQ, Liu XH (2014) Simultaneous determination of dihydroxybenzene isomers based on thionine functionalized multiwall carbon nanotubes modified electrode. *J Appl Electrochem* 44:667–674. doi:10.1007/s10800-014-0674-2
- Inam R, Bilgin C (2013) Square wave voltammetric determination of methiocarb insecticide based on multiwall carbon nanotube paste electrode. *J Appl Electrochem* 43:425–432. doi:10.1007/s10800-013-0526-5



26. Xu SJ, Zhang SM, Zhang JX, Tan T, Liu Y (2014) A maize-like FePO<sub>4</sub>@MCNT nanowire composite for sodium-ion batteries via a microemulsion technique. *J Mater Chem A* 2:7221–7228. doi:10.1039/c4ta00239c
27. Liu ZX, Deng HQ, Mukherjee PP (2015) Evaluating pristine and modified SnS<sub>2</sub> as a lithium-ion battery anode: a first-principles study. *ACS Appl Mater Interfaces* 7:4000–4009. doi:10.1021/am5068707
28. Zhong HX, Zhou P, Yue L, Tang DP, Zhang LZ (2014) Micro/nano-structured SnS<sub>2</sub> negative electrodes using chitosan derivatives as water-soluble binders for Li-ion batteries. *J Appl Electrochem* 44:45–51. doi:10.1007/s10800-013-0590-x
29. Li J, Yang ZJ, Tang Y, Zhang YC, Hu XY (2013) Carbon nanotubes–nanoflake-like SnS<sub>2</sub> nanocomposite for direct electrochemistry of glucose oxidase and glucose sensing. *Biosens Bioelectron* 41:698–703. doi:10.1016/j.bios.2012.09.059
30. Wang Z, Luan D, Madhavi S, Hu Y, Lou XW (2012) Assembling carbon-coated  $\alpha$ -Fe<sub>2</sub>O<sub>3</sub> hollow nanohorns on the CNT backbone for superior lithium storage capability. *Energy Environ Sci* 5:5252–5256. doi:10.1039/C1EE02831F
31. Sun HY, Ahmad M, Luo J, Shi YY, Shen WC, Zhu J (2014) SnS<sub>2</sub> nanoflakes decorated multiwalled carbon nanotubes as high performance anode materials for lithium-ion batteries. *Mater Res Bull* 49:319–324. doi:10.1016/j.materresbull.2013.09.005
32. Jin MC, Ren YP, Chen XH (2007) Determination of 6-benzyladenine in bean sprout by LC–ESI–IT–MS–MS. *Chromatographia* 66:407–410. doi:10.1365/s10337-007-0311-x
33. Yang L, Yan XP, Wang QW, Wang Q, Xia H (2015) One-pot catalytic conversion of cellulose into polyols with Pt/CNTs catalysts. *Carbohydr Res* 404:87–92. doi:10.1016/j.carres.2014.12.001
34. Liu H, Su Y, Chen P, Wang Y (2013) Microwave-assisted solvothermal synthesis of 3D carnation-like SnS<sub>2</sub> nanostructures with high visible light photocatalytic activity. *J Mol Catal A* 378:285–292. doi:10.1016/j.molcata.2013.06.021
35. Gong J, Liu J, Jiang ZW, Wen X, Mijowska E, Tang T, Chen XC (2015) A facile approach to prepare porous cup-stacked carbon nanotube with high performance in adsorption of methylene blue. *J Colloid Interface Sci* 445:195–204. doi:10.1016/j.jcis.2014.12.078
36. Hai B, Tang KB, Wang CR, An CH, Yang Q, Shen GZ, Qian YT (2001) Synthesis of SnS<sub>2</sub> nanocrystals via a solvothermal process. *J Cryst Growth* 225:92–95. doi:10.1016/S0022-0248(01)01030-2
37. Wang Q, Paim LL, Zhang XH, Wang SF, Stradiotto NR (2014) An electrochemical sensor for reducing sugars based on a glassy carbon electrode modified with electropolymerized molecularly imprinted poly-*o*-phenylenediamine film. *Electroanalysis* 26:1612–1622. doi:10.1002/elan.201400114